Journal of Power Sources 193 (2009) 878–884

Contents lists available at ScienceDirect

Journal of Power Sources

journal homepage: www.elsevier.com/locate/jpowsour

An inexpensive and efficient pyridine-based additive for the electrolyte of dye-sensitized solar cells

Jifu Shi, Bo Peng, Juan Pei, Shengjie Peng, Jun Chen*

Institute of New Energy Material Chemistry and Key Laboratory of Energy-Material Chemistry (Tianjin), Nankai University, Tianjin 300071, People's Republic of China

ARTICLE INFO

Article history:
Received 17 January 2009
Received in revised form 24 March 2009
Accepted 31 March 2009
Available online 8 April 2009

Keywords:
Dye-sensitized solar cells
Additive
Light-to-electricity conversion efficiency
Electrochemical impedance spectroscopy
Cyclic voltammetry

ABSTRACT

We report on the synthesis and application of an inexpensive pyridine-based additive allyl isonicotinate (AIN) for the efficient dye-sensitized solar cells (DSCs). AIN can be quickly synthesized at room temperature without any solvent. The presence of AIN in the electrolyte enhances the open-circuit voltage (V_{oc}), fill factor (FF) and short-circuit photocurrent (J_{sc}), consequently improving the energy conversion efficiency (η) from 6.5% to 8.2%. The impedance experiments show that the adsorption of AIN leads to the negative shift of the conduction band edge of the dye-sensitized TiO_2 around 55 mV. The presence of AIN in the electrolyte can obviously suppress the recombination of the injected electrons, increasing the lifetime of electrons in the TiO_2. The negative shift of the conduction band edge and the suppression of the recombination of the injected electrons contribute to the higher power conversion efficiency.

1. Introduction

Dye-sensitized solar cells (DSCs) have been intensively studied over the past decade and regarded as a promising low-cost alternative to the conventional solid-state devices. An impressive light-to-electricity energy conversion efficiency (η) of 11% has been achieved at AM 1.5 [1]. However, the values of the open-circuit voltage (V_{oc}) and short-circuit photocurrent (J_{sc}) reported previously are still substantially below the theoretical maximum [2,3], limiting the further improvement of the energy conversion efficiency of the DSCs. Changing either the conduction band edge position of TiO_2 or the recombination rate by adsorption of organic additives on the surface of TiO_2 can strongly affect the V_{oc} and J_{sc} [4–8], consequently influencing the photovoltaic performance.

At present, one of the most successfully used organic additives is 4-*tert*-butylpyridine (TBP) [9,10]. For the pyridine derivative, the N atom has a lone pair electron, which is prone to interact with coordinatively unsaturated Ti species on the TiO_2 film through Ti ← N bonds [11,12]. Treatment of the TiO_2 surface with TBP or the addition of TBP in the electrolyte can increase the V_{oc} drastically. One of the reasons for this increase of V_{oc} is the shift of the TiO_2 conduction band edge toward negative potentials due to the adsorption of TBP [13]. On the other hand, both the suppression of the dark current at the TiO_2/electrolyte interface and the formation of molecular complexes between TBP and iodine also play important roles in the improvement of V_{oc} [12,14]. However, the increase of the V_{oc} generally accompanies with a significant drop in the photocurrent [5,15]. In the molecule of TBP, the *tert*-butyl group as an electron donating group increases the charge density of the nitrogen atom of the pyridine ring, which enhances the interaction between the nitrogen atoms and the Ti(IV) ions. It seems that for the pyridine-based additives the stronger the interaction is, the more negative shift of the conduction band edge there will be [16]. The negative shift of the conduction band edge is beneficial to the increase of the V_{oc}. However, if the negative shift is too much, the electron injection from the photoexcited dye into the conduction band of the TiO_2 becomes difficult, leading to the decrease of the photocurrent [5,15]. Moreover, TBP is expensive, which limits its further industrial application. Therefore, we expect to design a new pyridine-based additive to adjust the interaction between the N atom of pyridine ring and the Ti(IV) ions, making the negative shift of the conduction band edge of TiO_2 moderately. This moderate negative shift of the conduction band edge can increase the V_{oc} but does not affect the short-circuit photocurrent. In this paper, allyl isonicotinate (AIN), which has an electron withdrawing group, i.e. *p*-ester group, on the pyridine ring (Scheme 1), was synthesized by a simple method. The electrochemical impedance spectroscopy (EIS) experiments show that a 55 mV negative shift of the conduction band edge of the TiO_2 is achieved due to the adsorption of AIN. The adsorption of AIN can suppress the electron transfer from the TiO_2 to the I_3^- in the electrolyte effectively. Consequently, the V_{oc} and FF as well as

* Corresponding author. Tel.: +86 22 23506808; fax: +86 22 23506808.
E-mail address: chenabc@nankai.edu.cn (J. Chen).

0378-7753/$ – see front matter © 2009 Elsevier B.V. All rights reserved.
doi:10.1016/j.jpowsour.2009.03.068

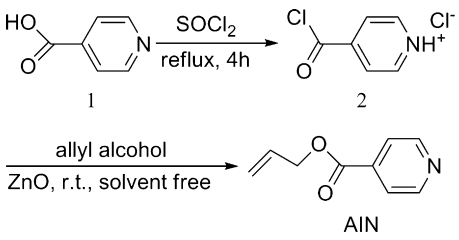

Scheme 1. Synthetic pathway of AIN.

the J_{sc} were enhanced greatly, leading to higher energy conversion efficiency.

2. Experimental

2.1. Synthesis and characterization

The starting materials are analytical grade (from Jinhua company of China). The synthetic pathway of the AIN is shown in Scheme 1. The isonicotinic acid chloride hydrochloride (**2**) was synthesized according to ref [17]. Briefly, 40 mL of $SOCl_2$ was added slowly from a dropping funnel on 20 g of isonicotinic acid (**1**) in an ice bath. The resulting solution was refluxed for 4 h and excess $SOCl_2$ was evaporated to dryness under reduced pressure at room temperature to obtain **2**. The crude product was washed with diethyl ether and dried in vacuum at 40 °C. Yield: 27.6 g (96%) of white crystals sufficiently pure for the preparation. ^{1}H NMR (300 MHz, DMSO-d_6): δ (ppm) 8.27 (d, J = 7 Hz, 2H), 9.04 (d, J = 7 Hz, 2H), 9.9 (b, 1H).

To a mixture of ZnO (3.04 g) and **2** (14 g) (without solvent), distilled allyl alcohol (5 mL) was added with a mechanical stirrer for 30 min at room temperature. The mixture was then eluted with CH_2Cl_2 (20 mL), and the CH_2Cl_2 extract was washed with an aqueous solution of sodium bicarbonate and dried over anhydrous sodium sulfate [18]. The product was obtained after solvent evaporation (yield: 9.5 g, 80%). Characterization: ^{1}H NMR (300 MHz, $CDCl_3$): δ (ppm) 4.85 (d, J = 6.8 Hz, 2H), 5.32 (d, J = 12 Hz, 1H), 5.42 (d, J = 19 Hz, 1H), 6.02 (m, 1H), 7.88 (d, J = 6 Hz, 2H), 8.79 (d, J = 6 Hz, 2H). ESI-MS: m/z 164 ([M + H]$^+$). Anal. Calcd. for $C_9H_9NO_2$: C 66.25%, N 8.58%, H 5.56%; found: C 66.28%, N 8.54%, H 5.65%.

From the synthesis process described above, it can be seen that AIN can be quickly synthesized at room temperature without any solvent, while ZnO can be re-used after simple washing with CH_2Cl_2 [18]. Thus, AIN can be obtained more economically.

2.2. The assembly of DSCs

The TiO_2 electrode was prepared by printing the TiO_2 paste (P25, Degussa AG, Germany) on the conductive glass of fluorine-doped SnO_2 (FTO, 20 Ω sq^{-1}, Wanyelong Company of China) [6]. The prepared TiO_2 film (thickness around 14 μm) was calcined at 450 °C for 30 min under flowing oxygen. Adsorption of the dye on the TiO_2 surface was done by soaking the TiO_2 electrodes in a dry ethanol solution of the dye *cis*-dithiocyanate-*N*,*N*′-bis(4,4′-dicarboxylate-2,2′-bipyridine)ruthenium(II) (N3) (standard concentration 3×10^{-4} M) at room temperature for 24 h. The Pt counter electrode was prepared by spin-coating H_2PtCl_6 solution (50 mM in isopropanol) onto FTO glass and sintering at 390 °C for 0.5 h [19].

Two types of electrolytes were employed in our experiments. Electrolyte A was composed of 0.6 M 1,2-dimethyl-3-propylimidazolium iodide (DMPImI), 0.1 M LiI, 0.05 M I_2, and acetonitrile as a solvent. Electrolyte B was obtained by adding 0.65 M AIN to electrolyte A. An enhancement of the η was observed when AIN was introduced into electrolyte A. However, when the concentration of AIN exceeds 0.65 M, the further improvement of η is not obvious. Therefore, the concentration of AIN is selected as 0.65 M. The DSCs were made by sealing the electrolytes between the dye-covered TiO_2 electrodes and the Pt counter electrodes.

2.3. Instruments and measurements

^{1}H NMR spectra were carried out by Varian Mercury Vx300 at 300 MHz with chemical shifts against TMS. ESI-MS data were measured with LCQ AD (Thermofinnigan, USA) mass spectrometer. The elemental analysis was performed by Vanio-EL (Heraeus). The absorption spectrum was measured by Jasco V-550 UV–vis spectrophotometer. FT-IR spectrum of pure AIN was recorded on a Bio-Rad FTS 135 FT-IR spectrometer using KBr discs; while the FT-IR spectrum of AIN-loaded TiO_2 film was tested using the way of 30° reflection.

The ionic conductivity (σ) of the electrolyte was determined by impedance measurement. The electrolyte was sandwiched between two mirror-finished stainless steel electrodes using a Teflon ring spacer in a constant volume cylindrical cell and was sealed with paraffin in the glove box. The conductivity was calculated from the ionic resistance (R), which was obtained from the intercept on the real part of the impedance in the complex plane (Fig. 1), by the following equation: $\sigma = K_{cell}/R$. The cell constant (K_{cell}) was 1.13 cm^{-1} determined by 0. 1 M KCl aqueous solution.

Impedance and voltammetry experiments were performed on a computer-controlled PARSTAT 2273 Advanced Electrochemical System (Princeton Applied Research) at room temperature in the dark. The EIS measurements were carried out in the frequency range from 100 kHz to 50 mHz with an amplitude of 10 mV. Cyclic voltammetry used to study the surface passivation effect of AIN was performed in 0.1 M tetrabutylammonium perchlorate acetonitrile solution containing 0 M or 0.65 M AIN. The working electrode was the TiO_2 film covered with N3. A platinum wire and Ag/$AgNO_3$ electrode were used as the counter and the reference electrode, respectively. The photocurrent–voltage (I–V) characteristics of DSCs were measured by a Keithley 2400 digital source meter controlled by a computer. A 500 W xenon lamp was served as sunlight simulator in combination with a band-pass filter (400–800 nm) to remove ultraviolet and infrared radiation. Further calibration was carried out by a USB4000 plug-and-play miniature fiber optic spectrometer (Ocean Optics, USA). The measurement of the incident monochromatic photon-to-current conversion efficiency (IPCE) was performed by a similar data collecting system but under

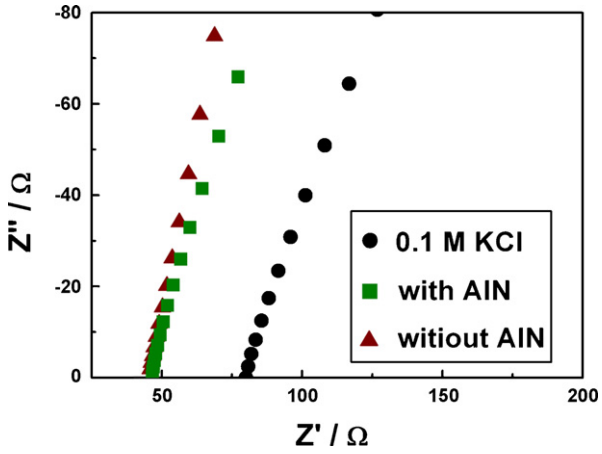

Fig. 1. The impedance spectra of 0. 1 M KCl aqueous solution (black circles), electrolyte A (without AIN, red triangles), and electrolyte B (with 0.65 M AIN, green squares) measured in a sandwiched cell assembled by two mirror-finished stainless steel electrodes. (For interpretation of the references to color in this figure legend, the reader is referred to the web version of the article.)

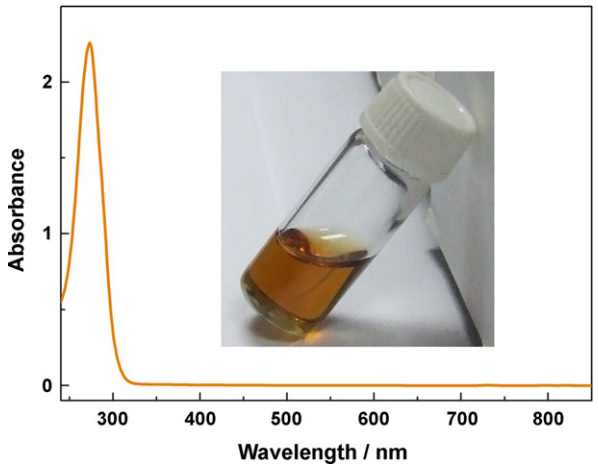

Fig. 2. Absorption spectrum of AIN in acetonitrile. The insert shows the photograph of the pure AIN in the glass bottle.

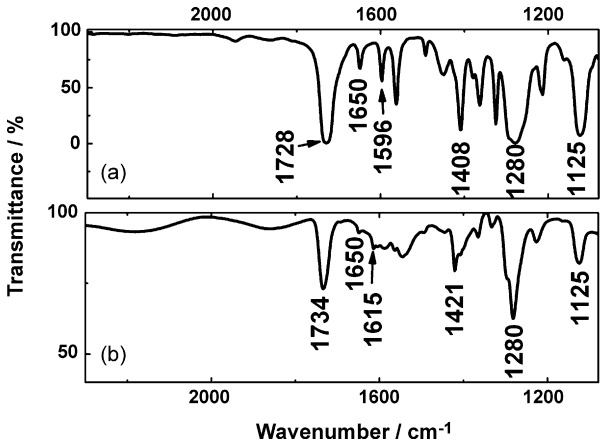

Fig. 3. The FT-IR spectra of (a) pure AIN and (b) AIN-loaded TiO_2 film.

monochromatic light, which was obtained by a grating spectrometer (SBP300, Zolix). The photocurrent action spectra were obtained by measuring the IPCE at different excitation wavelength with intervals of 10 nm.

3. Results and discussion

3.1. Spectra analysis

The as-synthesized AIN is orange liquid as shown in the insert of Fig. 2. The absorption peak of AIN in acetonitrile appears at 272 nm. This result indicates that, as an additive for the electrolyte, it does not affect the dye molecule to absorb the visible light.

Fig. 3a shows the FT-IR spectrum of the pure AIN. The 1728 cm^{-1} peak is assigned to ester carbonyl group stretching. The single at 1650 cm^{-1} is due to the C=C stretching band of the allyl; while the peaks at 1596 and 1408 cm^{-1} arise from the C=C stretching band of the pyridine moiety of AIN. The peaks centered at 1280 and 1125 cm^{-1} correspond to the C–O bands in the ester group. When the TiO_2 film was immersed in the 0.65 M AIN solution in acetonitrile (for 15 min and then fully rinsed with acetonitrile), the AIN was adsorbed on it. The FT-IR spectrum of this AIN-loaded TiO_2 film was shown in Fig. 3b. It is interesting to observe that the peaks arisen from pyridine moiety are shifted from 1596 to 1615 cm^{-1} and from 1408 to 1421 cm^{-1}, respectively, which is caused by the interaction between the N atoms and the unsaturated Ti species on the TiO_2 [20]. This interaction is further proved by the fact that the ester carbonyl group stretching is shifted from 1728 to 1734 cm^{-1}.

3.2. Cyclic voltammetry studies of the photoanode

Fig. 4a shows the cyclic voltammograms of the N3 covered TiO_2 films in 0.1 M tetrabutylammonium perchlorate acetonitrile solution (**1**) containing 0.65 M AIN and (**2**) without AIN. When an increasing negative potential is applied, a gradual onset of the cathodic current can be seen. The cathodic current in this CV measurement includes the capacitive current and the faradaic current [21]. For the TiO_2 film, there are a lot of surface states represented by coordinatively unsaturated Ti species. The capacitive current is caused by the capture of the injected electrons by the surface states of TiO_2 film [5]; while the faradaic current has relation to the electron transfer at the interface of TiO_2 and the electrolyte [21]. When the scan rate is high, the cathodic current is dominated by the capacitive current [21]. In our experiments, the scan rate is selected to be 0.8 V s^{-1}. The shapes of the obtained cyclic voltammograms indicating the cathodic current were dominated by capacitive cur-

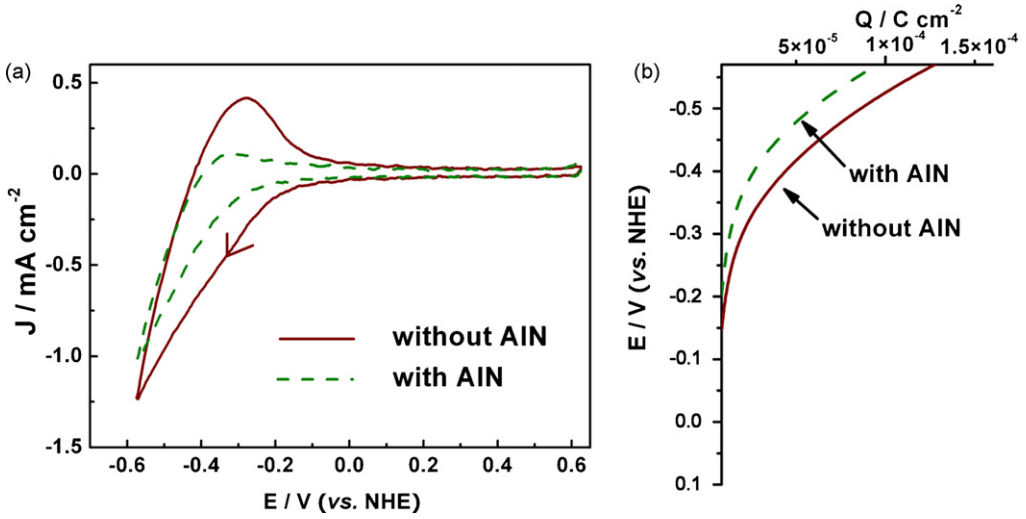

Fig. 4. (a) Cyclic voltammograms of N3 dye-covered TiO_2 electrodes in tetrabutylammonium perchlorate acetonitrile solution containing 0.65 M AIN and without AIN. The scan rate is 0.8 V s^{-1} and the active area of the TiO_2 electrodes is 0.5 cm^2. (b) Energy levels at the interfaces of the mesoscopic TiO_2 and tetrabutylammonium perchlorate acetonitrile solution.

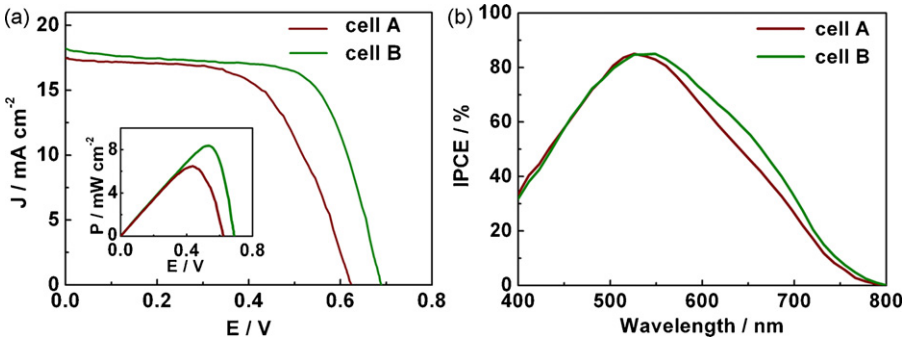

Fig. 5. (a) The photocurrent–voltage curves of cell A and cell B measured under 100 mW cm^{-2} illumination intensity. The power as a function of voltage for the two cells is depicted in the inset. (b) The photocurrent action spectra of cell A and cell B.

rent [5,21], despite the existence of a little section of the faradaic current. The coexistence of the faradaic current is a common phenomenon in the characterization of surface states of TiO_2 by CV method [5,21,22]. However, analysis of the cathodic current can still provide sufficient information to elucidate the passivation effect of additive on the TiO_2 surface states [5].

As shown in Fig. 4a, the much lower cathodic current is found with the presence of AIN in the solution, which implies that the number of the surface states is decreased due to the adsorption of AIN on the TiO_2 surface. For the reverse scans, the current approached zero at the more positive potentials, indicating that the injected negative charge is recovered. The injected charge can be expressed by [5]:

$$dQ = \frac{1}{\nu} I(V)\, dV \quad (1)$$

where Q is the injected charge, $I(V)$ is the current density, V is the potential applied on the electrode, and ν is the scanning rate. The integration of Eq. (1) gives the number of surface states vs the electrode potential as plotted in Fig. 4b. The Q increases much more slowly with the adsorption of AIN than that of without AIN under increasing forward bias due to better surface passivation, which is beneficial to improve the photovoltaic performance of DSCs.

3.3. Photovoltaic performance

Electrolyte A (without AIN) and electrolyte B (with 0.65 M AIN) were employed in the photovoltaic performance measurements. At 30 °C, the ionic conductivity of electrolyte A and electrolyte B are 24.6 and 24.2 mS cm^{-1}, respectively, calculated from Fig. 1 by the ionic resistance. This result indicated that the presence of AIN in the electrolyte almost unchanged the ionic conductivity. The photocurrent–voltage curves for the cells with electrolyte A (cell A) and electrolyte B (cell B) measured at a light intensity of 100 mW cm^{-2} are presented in Fig. 5a and the data are summarized in Table 1. The power vs voltage characteristics for the two cells are depicted in the inset. The J_{sc}, V_{oc}, and FF of cell A are 17.5 mA cm^{-2}, 0.62 V, and 0.60, yielding an overall η of 6.5%. The corresponding parameters (J_{sc}, V_{oc}, FF and η) of cell B with AIN as additive are 18.2 mA cm^{-2}, 0.69 V, 0.65, and 8.2%. Compared with that of electrolyte A, the addition of AIN enhances the η by 26% due to the increase of the J_{sc}, V_{oc}, and FF. The maximum powers, P_{max}, of cell A and cell B are 6.5 and 8.2 mW cm^{-2}, respectively.

Table 1
Parameters of photovoltaic performance for the cell A and cell B measured under 100 mW cm^{-2} illumination intensity.

Cell	J_{sc} (mA cm^{-2})	V_{oc} (V)	FF	P_{max} (mW cm^{-2})	η (%)
A	17.5	0.62	0.60	6.5	6.5
B	18.2	0.69	0.65	8.2	8.2

Fig. 5b is the photocurrent action spectra of cell A and cell B, in which the IPCE is plotted as a function of the excitation wavelength. The maximum IPCE of 85% was obtained at 530 nm for the both cells. It can be seen that the presence of AIN in the electrolyte broadened the photocurrent action spectrum, resulting in the higher J_{sc} of cell B as shown in Fig. 5a. The broadened photocurrent action spectrum is mainly caused by the lower back reaction rate of cell B at the TiO_2/electrolyte interface between the injected electrons and I_3^- due to the adsorption of AIN on the surface of TiO_2, which will be discussed in the following.

3.4. Electrochemical impedance spectroscopy and voltammetry studies of DSCs

The addition of AIN can enhance the performance of the DSCs distinctly, which can be explained in more detail in the electrochemical impedance spectroscopy. In order to elucidate the underlying electrokinetic process, the EIS were measured by varying the applied potential at equal intervals in the vicinity of V_{oc} (−0.37 to −0.72 V) in the dark. The shape of the impedance spectra is changed depending on the bias voltage. We took the electrochemical impedance spectra of cell A and cell B measured at moderate potential of −0.57 V (Fig. 6) just as an example to illustrate the relationship between the arcs of the EIS and the electrokinetic parameters of the DSCs. The fitting results of EIS measured from −0.37 to −0.72 V were depicted in Fig. 7. In Fig. 6, the larger semi-

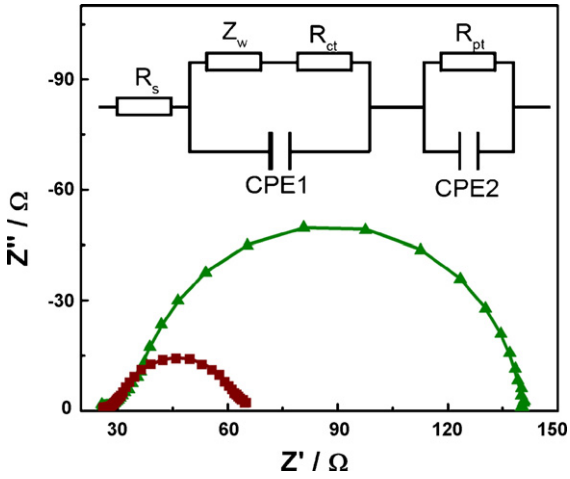

Fig. 6. Electrochemical impedance spectra of cell A (red squares) and cell B (green triangles) measured in the dark at −0.57 V. The lines show the fitted results. Equivalent circuit used for the curve fitting of the impedance spectra is shown in the inset. (For interpretation of the references to color in this figure legend, the reader is referred to the web version of the article.)

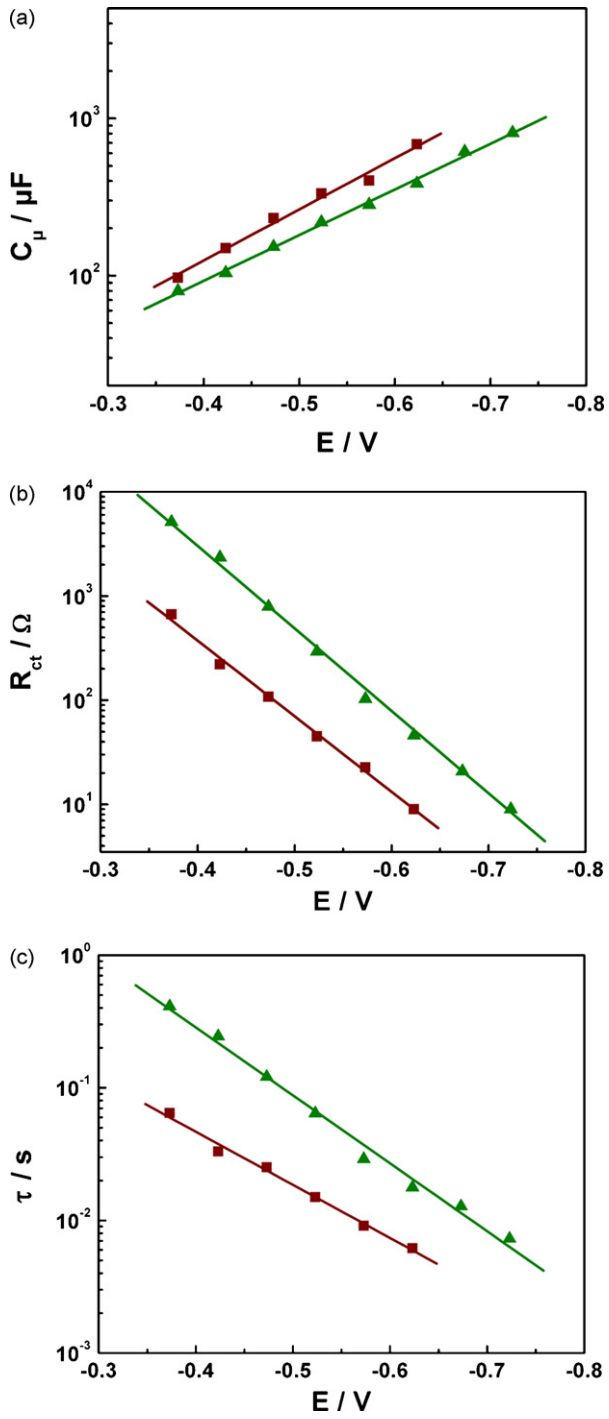

Fig. 7. Fitting results of (a) capacitance, (b) charge-transfer resistance, and (c) electron lifetime, cell A (red squares), cell B (green triangles). (For interpretation of the references to color in this figure legend, the reader is referred to the web version of the article.)

circle at intermediate frequencies (~100–1 Hz) is mainly attributed to the charge-transfer at the TiO_2/electrolyte interface [23]. It can be seen that this charge-transfer resistance of cell B is larger than that of cell A due to the presence of the AIN.

The inset of Fig. 6 presents the equivalent circuit used for the curve fitting of the impedance spectra [24]. Good agreement between the measured and the fitted data is achieved in all cases. R_s includes the ohmic resistance of the electrolyte, the FTO substrate, and the contact wires. The electron transport resistance in the TiO_2 can be described by Warburg diffusion impedance Z_W. R_{ct} is the charge-transfer resistance at the TiO_2/electrolyte interface. CPE1 is the chemical capacitance produced by the accumulation of electrons in the film. The impedance of the CPE is given by: $Z_{CPE} = B(i\omega)^{-m}$, where ω is the angular frequency, B is the CPE parameter, and m ($0 \leq m \geq 1$) is the CPE exponent [19,25]. For an ideal capacitance the CPE exponent is 1 and in our experiments the CPE exponent is about 0.95, which indicates that the deviation from an ideal capacitance is small [25]. Thus, the constant phase element CPE1 can be replaced by a capacitive element C_μ. R_{pt} is the charge-transfer impedance at the counter electrode and CPE_2 is the double layer capacitance (C_{pt}) at the electrolyte/Pt-FTO interface.

Table 2
The fitting results of EIS parameters for the DSCs of cell A and cell B and electrochemical cells of C, D and E measured under −0.57 V in the dark.

Cell[a]	R_s (Ω)	R_{ct} (Ω)	C_μ (μF)	R_{pt} (Ω)	C_{pt} (μF)
A	25.9	22.7	403.2	3.7	42.6
B	26.1	102.8	283.0	3.9	40
C	25.2	21.3	126.7	4.1	49
D	26.3	51.3	122.8	3.8	56
E	27.6	92.2	70.3	4.3	47.1

[a] Cell A and cell B are DSCs with the electrolyte contained 0 M (cell A) or 0.65 M (cell B) AIN; while cell C, cell D and cell E are electrochemical cells (without adsorption of N3 on the TiO_2 film) with electrolyte contained 0 M (cell C), 0.3 M (cell D), and 0.65 M (cell E) AIN. The active area of the cells is 0.16 cm^{-2}.

The parameters from the fitting procedure of Fig. 6 are presented in Table 2. It can be seen the presence of AIN has obvious effect on the R_{ct} and C_μ. However, the parameters of R_s, R_{pt}, and C_{pt} are not sensitive to the addition of AIN because the AIN mainly influences the electron transfer process occurred at the interface between TiO_2 and electrolyte by adsorption. Thus, we emphasize on the changes of R_{ct} and C_μ of cell A and cell B in the following.

The fitting results of C_μ at different potentials are plotted in Fig. 7a. C_μ follows a characteristic exponential rise with increasing forward bias given by [5]:

$$C_\mu = C_a \exp\left[\frac{-\alpha eV}{k_B T}\right] + C_b \quad (2)$$

where C_a is the prefactor of the exponential increase, e is the elementary charge, V is the applied potential, k_B is the Boltzmann constant, T is the temperature, C_b is the quasi-constant capacitance at low potentials, and α is a coefficient describing either the Boltzmann occupancy of the conduction band capacitance ($\alpha = 1$) or an exponential distribution of trap states ($\alpha < 1$) [5]. In our measurements, α is calculated to be 0.19 for cell A and 0.17 for cell B, respectively, which are in agreement with the reported 0.17–0.24 [5]. The adsorption of pyridine derivative passivates the surface states and induces a negative conduction band edge movement. That is why the values of C_μ of cell B are lower than that of cell A as shown in Fig. 7a [5], and this tendency is consistent with the cyclic voltammograms results above. The difference of the potential at the same value of C_μ can indicate the shift of the conduction band edge [23]. The adsorption of AIN leads to around 55 mV negative shift of the conduction band edge, which is much lower than that of TBP (160 mV) [13].

The R_{ct} values of cell A and cell B are shown in Fig. 7b. The adsorption of AIN on the surface of TiO_2 reduces the number of recombination centers and limits the charge losses, leading to higher R_{ct} values for cell B. At moderate potentials, R_{ct} follows the Buttler-Volmer relationship given by [23]:

$$R_{ct} = R_0 \exp\left[-\frac{\beta}{k_B T}(E_F - E_r)\right] \quad (3)$$

where E_F is the position of the Fermi level of electrons, E_r is the energy of the redox couple, β is the transfer coefficient, and R_0 is a constant. The β of cell A and cell B are calculated to be 0.43 and

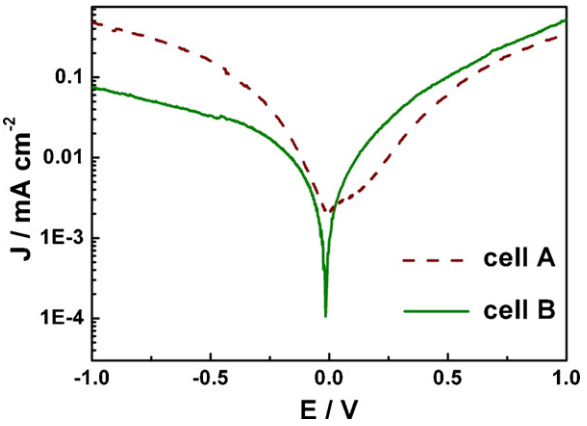

Fig. 8. The linear sweep voltammograms of cell A and cell B measured in the dark. The scan rate is 0.01 V s^{-1}.

0.48 respectively, which is close to the previously reported value of $\beta = 0.5$ [26].

The improvement of V_{oc} can therefore be ascribed to a combined effect of the negative shift of conduction band edge and the limitation of charge losses due to that the V_{oc} is determined by the difference between the quasi-Fermi level of TiO_2 and the potential of the redox couple in the electrolyte. The negative shift of the conduction band edge and the limitation of the charge losses augment the quasi-Fermi level of the conduction band electrons in the TiO_2 film and then increase the V_{oc} of cell B.

The product of R_{ct} and C_μ corresponds to the electron lifetime, $\tau = R_{ct} \times C_\mu$, which is shown in Fig. 7c. With increasing forward bias, τ for both cells decreases, which is due to the augmentation of the concentration of injected electrons in the film. The evident characteristic in Fig. 7c is that the τ of cell B is much larger than that of cell A, which is one of the reasons why the photovoltaic performance of cell B is superior to that of the cell A. The increase in τ is associated with a pronounced rise in the charge-transfer resistance.

Another distinct effect of AIN is to enhance the photocurrent. For a given DSC, the photocurrent is determined by the following two processes: (1) The photoexcited dye molecules inject electrons into the conduction band of the TiO_2. (2) The injected electrons are extracted from the nanocrystalline to the outer electrical circuit to form the photocurrent. Too much negative shift of the conduction band hampers the electron injection from the excited sensitizer, that is why the adsorption of TBP always induces a drop in the photocurrent [5,15]. However, the presence of AIN enhances the J_{sc} from 17.5 to 18.2 mA cm^{-2}. The increase of the J_{sc} indicates that the electron injection process is not affected by the slightly negative shift of the conduction band edge. This result is in keeping with the previous report, in which it has been concluded that if the negative shift of the conduction band edge is small enough (around 50 mV), the electron injection is not hindered [5]. The adsorption of AIN leads to a 55 mV shift of the conduction band edge and does not hamper the injection of the electrons. Thus, the process (2), i.e. the charge extraction efficiency of the injected electrons, is decisive to the photocurrent of the cell. Suppression the recombination is beneficial to increase the photocurrent. The relation between the photocurrent (J_{ph}) and the surface recombination current (J_r) can be expressed as $J_{ph} = J_{inj} - J_r$ [3], and J_{inj} is the electron injection current resulting from dye. J_r can be estimated from the dark current [5,27]. Fig. 8 shows the dark current of cell A and cell B measured in the dark with a scan rate of 0.01 V s^{-1}. When a negative potential was applied, the I_3^- was reduced to I^- at the TiO_2/electrolyte interface. As far as the operation of the DSC is concerned, this process corresponds to the recombination of the injected electrons with I_3^-. Fig. 8 clearly shows that the dark current of cell A is higher than that of the cell B in the negative potential range. On condition that the J_{inj} is equal for cell A and cell B, the lower dark current of cell B results in the higher photocurrent, which is in keeping with the broadened photocurrent action spectrum shown in Fig. 5b.

With the addition of AIN in the electrolyte, the FF is increased from 0.60 to 0.65. The better FF has relation to the higher transfer coefficient β of electron transfer from TiO_2 to the electrolyte [23]. For cell A, the β is 0.43 and for cell B the β is 0.48. The higher FF of cell B compared with that of cell A is partly caused by the relatively higher β.

3.5. Isolated effect of AIN on the shift of conduction band edge

As mentioned above, the adsorption of AIN on the dye-covered TiO_2 film caused a negative shift of the conduction band edge. However, the adsorption of ruthenium complexes-based dyes can induce a positive shift of the conduction band edge due to the transfer of protons of the dyes to the surface of TiO_2 [28,29]. In order to better understand the isolated effect of AIN on the conduction band edge shift, more systematical study employing electrochemical cells (without dye adsorbed on TiO_2) and electrolytes with different concentration of AIN (0.00 M, 0.30 M, and 0.65 M) was carried out. The EIS of electrochemical cell C (0.00 M AIN), cell D (0.30 M AIN), and cell E (0.65 M AIN) were measured by varying the applied potential at equal intervals ranging from −0.47 to −0.72 V in the dark.

As an example, the impedance spectra of electrochemical cell C, cell D, and cell E measured at −0.57 V were shown in Fig. 9a. The parameters from the fitting procedure of Fig. 9a are also presented in Table 2. The parameters of R_s, R_{pt}, and C_{pt} are not obviously changed of the three cells for the same reason mentioned above.

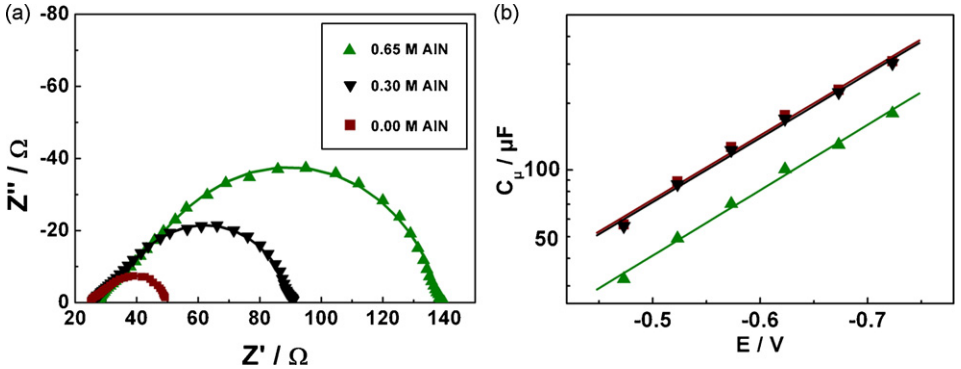

Fig. 9. (a) Electrochemical impedance spectra of cell C (without AIN, red squares), cell D (0.3 M AIN, black inverted triangles), and cell E (0.65 M AIN, green triangles) measured in the dark at −0.57 V. (b) Fitting results of capacitance of the three cells. (For interpretation of the references to color in this figure legend, the reader is referred to the web version of the article.)

It can be seen that the R_{ct} was increased with the increase of AIN concentration, which is reasonable because the increase of AIN concentration could decrease the number of electron transfer centers from TiO_2 to I_3^-. In the following, we emphasize on the changes of the C_μ of the three cells to elucidate the isolated effect of AIN on the conduction band edge shift.

The fitting results of C_μ of the three cells are depicted in Fig. 9b. No significant difference is found between cell C and cell D, indicating that the addition of 0.3 M AIN has slightly effect on the negative shift of the conduction band edge. This phenomenon is probably because of the weak interaction between the AIN and TiO_2. To induce an obvious negative shift of the conduction band edge of TiO_2, a higher concentration of AIN is necessary. For cell E with 0.65 M AIN in the electrolyte, the C_μ values are decreased, indicating an 80 mV negative shift of the conduction band edge compared with that of cell C without AIN.

For the N3-coated TiO_2 film, the presence of 0.65 M AIN caused a 55 mV negative shift of the conduction band edge (see Fig. 7a), which is lower than that of 80 mV without adsorption of dye. In addition, compared cell C (without N3 and AIN) with cell A (with N3, without AIN), it can be found that the adsorption of N3 leads to a 200 mV positive shift of the conduction band edge.

The effect of AIN on the negative shift of the conduction band edge is further studied by theoretical calculations. The preliminary results also display that the conduction band edge of TiO_2 is negatively shifted after adsorption of AIN. More detailed calculation is under way.

4. Conclusions

An inexpensive pyridine derivative AIN was synthesized through a simple method at room temperature. Our experiments show that the addition AIN into the electrolyte could remarkably enhance the light-to-electricity conversion efficiency. The adsorption of AIN on the TiO_2 induces a negative shift of the conduction band edge. The moderate shift of the conduction band edge of TiO_2 nanocrystals, as well as the inhibition of dark current from TiO_2 to the triiodide in the electrolyte contributes to the higher energy conversion efficiency. This work should be useful for the manufacturing of low-cost and high-efficiency DSCs.

Acknowledgements

This work was supported by the Programs of National 973 (2005CB623607) and Tianjin High-Tech (07ZCGHHZ00700).

References

[1] M. Grätzel, J. Photochem. Photobiol. A 164 (2004) 3–14.
[2] G. Smestad, Sol. Energy Mater. Sol. Cells 32 (1994) 273–288.
[3] S.Y. Huang, G. Schlichthorl, A.J. Nozik, M. Grätzel, A.J. Frank, J. Phys. Chem. B 101 (1997) 2576–2582.
[4] T.S. Kang, K.H. Chun, J.S. Hong, S.H. Moon, K.J. Kim, J. Electrochem. Soc. 147 (2000) 3049–3053.
[5] Z. Zhang, S.M. Zakeeruddin, B.C. O'Regan, R. Humphry-Baker, M. Grätzel, J. Phys. Chem. B 109 (2005) 21818–21824.
[6] W. Xu, J. Pei, J. Shi, S. Peng, J. Chen, J. Power Sources 183 (2008) 792–798.
[7] J.H. Park, K.J. Choi, J. Kim, Y.S. Kang, S.S. Lee, J. Power Sources 173 (2007) 1029–1033.
[8] T. Kato, M. Fujimoto, T. Kado, S. Sakaguchi, D. Kosugi, R. Shiratuchi, W. Takashima, K. Kaneto, S. Hayase, J. Electrochem. Soc. 152 (2005) A1105–A1108.
[9] M.K. Nazeeruddin, A. Kay, I. Rodicio, R. Humphry-Baker, E. Mueller, P. Liska, N. Vlachopoulos, M. Grätzel, J. Am. Chem. Soc. 115 (1993) 6382–6390.
[10] K.S. Ahn, S.J. Yoo, M.-S. Kang, J.W. Lee, Y.E. Sung, J. Power Sources 168 (2007) 533–536.
[11] H. Kusama, H. Orita, H. Sugihara, Langmuir 24 (2008) 4411–4419.
[12] C. Shi, S. Dai, K. Wang, X. Pan, F. Kong, L. Hu, Vib. Spectrosc. 39 (2005) 99–105.
[13] G. Boschloo, L. Häggman, A. Hagfeldt, J. Phys. Chem. B 110 (2006) 13144–13150.
[14] H. Greijer, J. Lindgren, A. Hagfeldt, J. Phys. Chem. B 105 (2001) 6314–6320.
[15] K.-M. Lee, V. Suryanarayanan, K.C. Ho, J. Power Sources 185 (2008) 1605–1612.
[16] H. Kusama, H. Arakawa, Sol. Energy Mater. Sol. Cells 81 (2004) 87–99.
[17] K.I. Nättinen, K. Rissanen, Cryst. Growth Des. 3 (2003) 339–353.
[18] M.H. Sarvari, H. Sharghi, Tetrahedron 61 (2005) 10903–10907.
[19] F. Cai, J. Liang, Z. Tao, J. Chen, R. Xu, J. Power Sources 177 (2008) 631–636.
[20] K. Hara, Y. Dan-oh, C. Kasada, Y. Ohga, A. Shinpo, S. Suga, K. Sayama, H. Arakawa, Langmuir 20 (2004) 4205–4210.
[21] F. Fabregat-Santiago, I. Mora-seró, G. Garcia-Belmonte, J. Bisquert, J. Phys. Chem. B 107 (2003) 758–768.
[22] S. Wu, H. Han, Q. Tai, J. Zhang, S. Xu, C. Zhou, Y. Yang, H. Hu, B. Chen, X.Z. Zhao, J. Power Sources 182 (2008) 119–123.
[23] Q. Wang, S. Ito, M. Grätzel, F. Fabregat-Santiago, I. Mora-Seró, J. Bisquert, T. Bessho, H. Imai, J. Phys. Chem. B 110 (2006) 25210–25221.
[24] Q. Wang, J.E. Moser, M. Grätzel, J. Phys. Chem. B 109 (2005) 14945–14953.
[25] A. Hauch, A. Georg, Electrochim. Acta 46 (2001) 3457–3466.
[26] F. Fabregat-Santiago, J. Bisquert, G. Garcia-Belmonte, G. Boschloo, A. Hagfeldt, Sol. Energy Mater. Sol. Cells 87 (2005) 117–131.
[27] D.B. Menzies, Q. Dai, Y.-B. Cheng, G.P. Simon, L. Spiccia, C. R. Chimie 9 (2006) 713–716.
[28] F.D. Angelis, S. Fantacci, A. Selloni, M. Grätzel, M.K. Nazeeruddin, Nano Lett. 7 (2007) 3189–3195.
[29] M.K. Nazeeruddin, R. Humphry-Baker, P. Liska, M. Grätzel, J. Phys. Chem. B 107 (2003) 8981–8987.